NANO LETTERS

Letter

pubs.acs.org/NanoLett

Transparent Triboelectric Nanogenerators and Self-Powered Pressure Sensors Based on Micropatterned Plastic Films

Feng-Ru Fan,[†,‡,∥] Long Lin,[†,∥] Guang Zhu,[†,∥] Wenzhuo Wu,[†] Rui Zhang,[†] and Zhong Lin Wang*[,†,§]

[†]School of Material Science and Engineering, Georgia Institute of Technology, Atlanta, Georgia 30332-0245, United States

[‡]State Key Laboratory of Physical Chemistry of Solid Surfaces, Department of Chemistry, College of Chemistry and Chemical Engineering, Xiamen University, Xiamen 361005, China

[§]Beijing Institute of Nanoenergy and Nanosystems, Chinese Academy of Sciences, Beijing, China

Supporting Information

ABSTRACT: Transparent, flexible and high efficient power sources are important components of organic electronic and optoelectronic devices. In this work, based on the principle of the previously demonstrated triboelectric generator, we demonstrate a new high-output, flexible and transparent nanogenerator by using transparent polymer materials. We have fabricated three types of regular and uniform polymer patterned arrays (line, cube, and pyramid) to improve the efficiency of the nanogenerator. The power generation of the pyramid-featured device far surpassed that exhibited by the unstructured films and gave an output voltage of up to 18 V at a current density of ~0.13 μA/cm^2. Furthermore, the as-prepared nanogenerator can be applied as a self-powered pressure sensor for sensing a water droplet (8 mg, ~3.6 Pa in contact pressure) and a falling feather (20 mg, ~0.4 Pa in contact pressure) with a low-end detection limit of ~13 mPa.

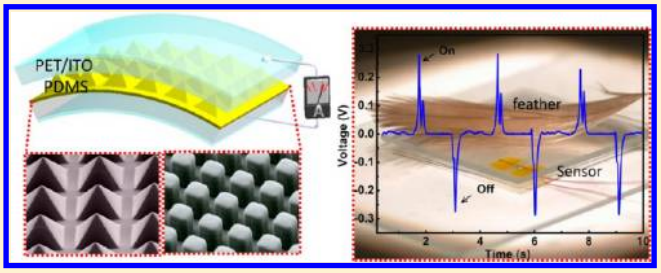

KEYWORDS: *Nanogenerator, transparent, polymer, pressure sensor*

The integration of flexible and transparent characteristics is an important component in the new organic electronic and optoelectronic devices[1−3] and has been achieved for various applications, including transistors,[4,5] lithium-ion batteries,[6] supercapacitors,[7,8] pressure sensors, and artificial skins.[9−12] Indeed, building flexible transparent energy conversion and storage units plays a key role in realizing fully flexible and transparent devices. In 2006, our group demonstrated the first piezoelectric ZnO nanogenerator that successfully converted mechanical energy into electric energy.[13] Since then, various nanogenerators (NGs) based on piezoelectric effect have been demonstrated.[14−17] As an important part in this field, some studies on fully integrated flexible and transparent NGs have been reported.[18−21] Almost all of them are based on piezoelectric ZnO nanowires and the entire device requires sophisticated design and a high degree of integration.

The general physical process for energy conversion has three important steps: charge generation, charge separation, and charge flow. These steps were accomplished in piezoelectric NGs by employing the piezoelectric potential created under strain. Recently, we have developed a flexible triboelectric generator (TEG) using all-polymer based materials.[22] By stacking two thin polymer films made of Kapton and polyester (PET), a charge generation, separation, and induction process can be achieved through a mechanical deformation of the polymer films as a result of the triboelectric effect. This is a simple, low-cost, readily scalable fabrication process of generator that can convert random mechanical energy in our living environment into electric energy using the well-known triboelectric effect. Furthermore, through rational design, this new mode of power generation can be developed to build a high-output, flexible, and transparent NG.

To make the device transparent and improve the power generation density, three approaches were employed in this research: (i) replacing Kapton film with transparent PDMS film, (ii) replacing Au electrodes with transparent indium tin oxide (ITO) electrodes, then the entire structure is flexible and transparent, and (iii) fabricating various PDMS pattern arrays to enhance the friction effect, resulting in a high-output generator (Supporting Information Figure S1). Furthermore, we show that such a device is also a powerful tool and can be used to detect the subtle pressure and vibration, such as the falling of a water droplet and very gentle touch of a feather on surfaces.

A TEG is made of two sheets of polymers that have distinctly different triboelectric characteristics with one easy to gain electrons and the other one easy to lose electrons.[22] By stacking the two sheets together with flexibility of relative sliding, two insulating polymeric materials are touched and rubbed with each other when deformed by an external mechanical deformation. Thus, triboelectric charges with opposite signs

Received: March 12, 2012
Revised: April 29, 2012

   dx.doi.org/10.1021/nl300988z | *Nano Lett.* XXXX, XXX, XXX−XXX

are generated and distributed on the internal surfaces of the two polymers. As soon as the deformation starts to be released, the opposite triboelectric charges become separated with an air gap and form a dipole moment. As a result, an electric potential difference is established between the two planar electrodes. To achieve equilibrium, electrons flow from the side with lower potential to that with higher potential, leading to accumulation of electrostatically inducted charges on the electrodes. If the deformation is then reapplied so that the two polymers are in contact, the dipole moment disappears or reduced in magnitude. Thus, the reduced electric potential difference leads to the electrons in the electrode to flow in the opposite direction, and thus the accumulated inducted charges vanish. Therefore, with repeated bending and releasing of the structures electrons are driven top flow through the external load in an alternating manner. This is the basic principle of the alternating current TEG (Supporting Information Figures S2 and S3).

Instead of using the relatively flat polymer sheets, we have fabricated some patterns on the polymer surfaces to increase the triboelectric power output. To make patterned polydimethylsiloxane (PDMS) films, Si wafer molds were first fabricated by traditional photolithography method, followed by dry or wet etching process to fabricate different recessed features including lines, cubes, and pyramids. The surface of the molds was initially treated with trimethylchlorosilane to prevent the PDMS film from sticking to the master. The liquid PDMS elastomer and cross-linker were mixed, degassed, and uniformly spin-coated on the surface of the master. After curing thermally, a uniform PDMS layer was peeled off and contained the inverse of the original pattern features on the surface of the mold. Finally, the PDMS film was fixed on the insulation surface of a clean ITO-coated polyester (PET) substrate by a thin PDMS bonding layer, and then the entire structure was covered with another ITO-coated PET film to form a sandwich-structured device. A detailed fabrication protocol and typical structure of a flexible transparent nanogenerator (FTNG) is schematically shown in Figure 1. One significant advantage of this technique is that hundreds of replicas of patterned PDMS films can be produced from one single mold. Silicon-based molds can be replaced by metal molds (Ni or Al) due to their excellent mechanical properties and longevity. The entire preparation process of the device is simple and low-cost, making it possible to be scaled-up for large-scale production and practical applications.

Optical and scanning electron microscopy (SEM) analysis of the resulting PDMS pattern arrays show that the above-mentioned fabrication protocol yields regular and uniform microstructures across the whole area of a 4 in. wafer mold (Figure 2). The shape and lateral dimensions of the polymer structure are well controlled by the initial patterns on the surface of the wafer mold. Here, we fabricated three kinds of PDMS pattern arrays, including lines, cubes, and pyramids. As shown in Figure 2A–C, the size of single PDMS features is limited to about 10 μm. Smaller features down to 5 μm were also produced with consistent quality (Supporting Information Figure S4). High-magnification SEM images illustrate that all of the features are regular and remarkably uniform, demonstrating that this procedure is an efficient method in preparing large-scale uniform plastic microstructures.[10,23] Importantly, each pyramid feature has a perfect geometric structure and a sharp tip, which is beneficial for increasing the friction area and the efficiency in the power generation process of the FTNG. In addition, the prepared PDMS film is stretchable and transparent, as illustrated in Figure 2D.

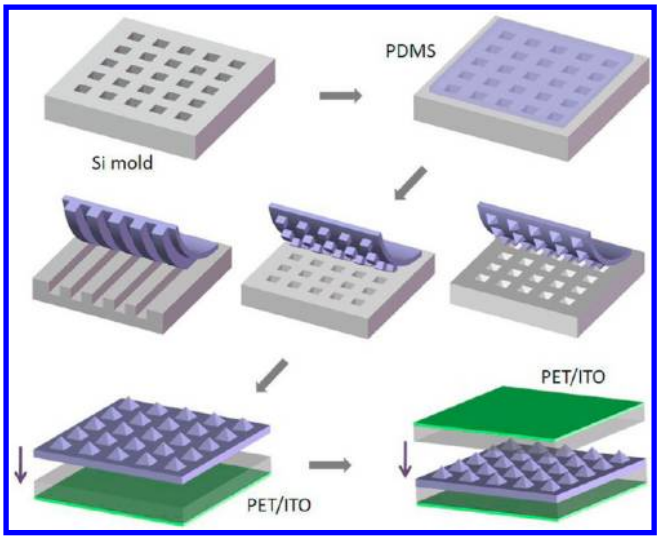

Figure 1. Schematic illustration of the fabrication process of the FTNG and the pressure sensor devices. The patterned (100) Si wafers serve as the mold for the fabrication of PDMS thin film with various features such as patterned lines, cubes, and pyramids. The FTNG and the pressure sensor devices were both composed of a sandwiched structure with two ITO-coated PET membranes and a layer of patterned PDMS thin film. The detailed description of the fabrication process is stated in the method session.

To investigate the electrical output performance of the polymer FTNG, we made a detailed comparative characterization of the devices with different PDMS features. Figure 3A,B shows the open-circuit voltage and short-circuit current output of the typical FTNGs with four different PDMS feature types: film (unstructured plane), line, cube, and pyramid. The result clearly shows that the order of the output efficiency of different FTNGs follows film < line < cube < pyramid. When we used a linear motor in a cyclic agitation to periodically bend and release FTNG (at a frequency of 0.33 Hz and with a strain of 0.13%), the maximum output voltage and current signal for pyramid-featured devices are up to 18 V and 0.7 μA (corresponding to a current density of 0.13 μA/cm^2), respectively, which are almost four times as high as the previously reported TEG using flat films and can also compare favorably with that received based on piezoelectric materials and complex designs. The dramatic increase in the electrical output of the structured films over the unstructured films can be attributed to the following factors: (1) the triboelectric effect of the microstructured films far surpassed that exhibited by the unstuctured films with similar thickness. A surface with more sophisticated structures has larger effective triboelectric effect and can generate more surface charges during the friction. (2) The capacitance change in the deformation process is significantly improved due to the presence of the air voids and the increase in effective dielectric constant.[10] (3) In the microstructured films, the triboelectric charges are more easily separated and thus a larger dipole moment will form between the electrodes. It has also been demonstrated that a completely sealed device with few air voids/bubbles and weak sliding shows a rather low output due to the weak friction. Therefore, the PDMS films with pyramid or cube structures in particular give almost 5–6 times improvement in the power generation compared with that in the unstructured films. It should be

dx.doi.org/10.1021/nl300988z | Nano Lett. XXXX, XXX, XXX–XXX

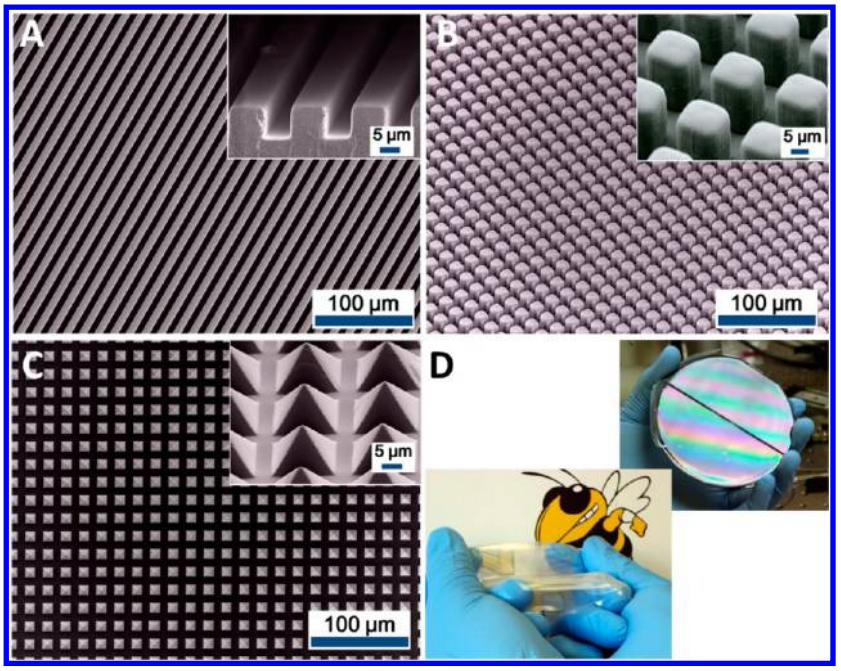

Figure 2. Structure characterization of the patterned PDMS thin film. (A) SEM image of the patterned PDMS thin film with line features. The inset is a 75°-tilted high magnification image showing the size and cross section structure of the features. (B) SEM image of the patterned PDMS thin film with cubic features. The inset is a 45°-tilted high-magnification image showing the height of the cubes. (C) SEM image of the patterned PDMS thin film with pyramids features. The inset is a 45°-tilted high-magnification image showing the pyramid structure of the features. (D) Photographs showing the appearance of the as-fabricated PDMS thin film. Top-right: the photograph of as-fabricated PDMS thin film on the Si mold. The interference fringes on the surface of the PDMS film indicate the uniform patterned features at large scale. Bottom-left: the peeled-off PDMS thin film showing its flexibility and transparency.

noted that when the size of the features is reduced to 5 μm from 10 μm, the output voltage of the generator has no obvious improvement. The possible reason is that the triboelectric effect did not increase significantly and the smaller features were more susceptible to defects as a result of imperfections in the Si mold.

The detailed power generation mechanism of the triboelctric generator has been illustrated in our previous report.[22] Generally, a triboelectric dipole layer induces the potential difference between the electrodes in a bending or releasing process, which will drive the free electrons to flow across the external load to countervail the field produced by the triboelectric changes (Figure 3C and Supporting Information Figure S2). The current I generated across an external load can be defined as follows

$$I = C\frac{\partial V}{\partial t} + V\frac{\partial C}{\partial t}$$

where C denotes the capacitance of the system and V is the voltage across the two electrodes. The first term is the variation in the potential across the top and bottom electrodes owing to the triboelectric charges. The second term is the change in the capacitance of the system as the distance between the top and bottom electrodes is changed due to the mechanical deformation of the unit. Therefore, the power generation performance of the FTNG is closely related to the capacitance change of the system. Hence, through rational design we have significantly improved its ability in the power generation utilizing polymer patterned arrays to increase the triboelectric effect and the capacitance change. Here, PDMS film plays an important role and benefits the performance in two aspects: (1) it is a soft, transparent material and could easily be fabricated into a patterned array with various features, (2) the location of PDMS in the triboelectric series is far away from that of PET, which is critical for achieving a higher performance (Supporting Information Figures S5 and S6). Furthermore, since the entire structure is based on polymer materials, the FTNG exhibits excellent mechanical robustness and stability, and it can still work properly after being tested for ~10^5 cycles (Figure 3D).

The goal of our design is to integrate flexible, high-output, and transparent properties into a single nanogenerator. To achieve the purpose of transparent devices, we therefore assembled the entire device with only two transparent polymer materials (PET and PDMS) and a transparent electrode material (ITO). To systematically characterize the transparency of FTNG components and the full devices with different PDMS patterns, UV−vis spectroscopy is used to study the transmittance of the devices, as shown in Figure 3E. The commercial ITO-coated PET film showed a transmittance of 85% in the visible and near-infrared region. After coated with a layer of unstructured PDMS film, the transmittance is almost unchanged. A full film-featured nanogenerator exhibits a high transmittance of ~75%. Since the microstructures have a strong light scattering effect, the other three full FTNGs with different PDMS features show a lower transmittance (approximately 50%). Figure 3F shows the photograph of a FTNG adhered on the screen of a smart phone, which indicates the high transparency of the FTNG and its potential application in touchscreen, high-definition LCD, and other self-powered electronic displays.

The FTNG device can itself generate a voltage or current output via deformation of two polymer sheets by external mechanical forces. This is the basic principle of the triboelectric generator and can be applied as a self-powered pressure

dx.doi.org/10.1021/nl300988z | Nano Lett. XXXX, XXX, XXX−XXX

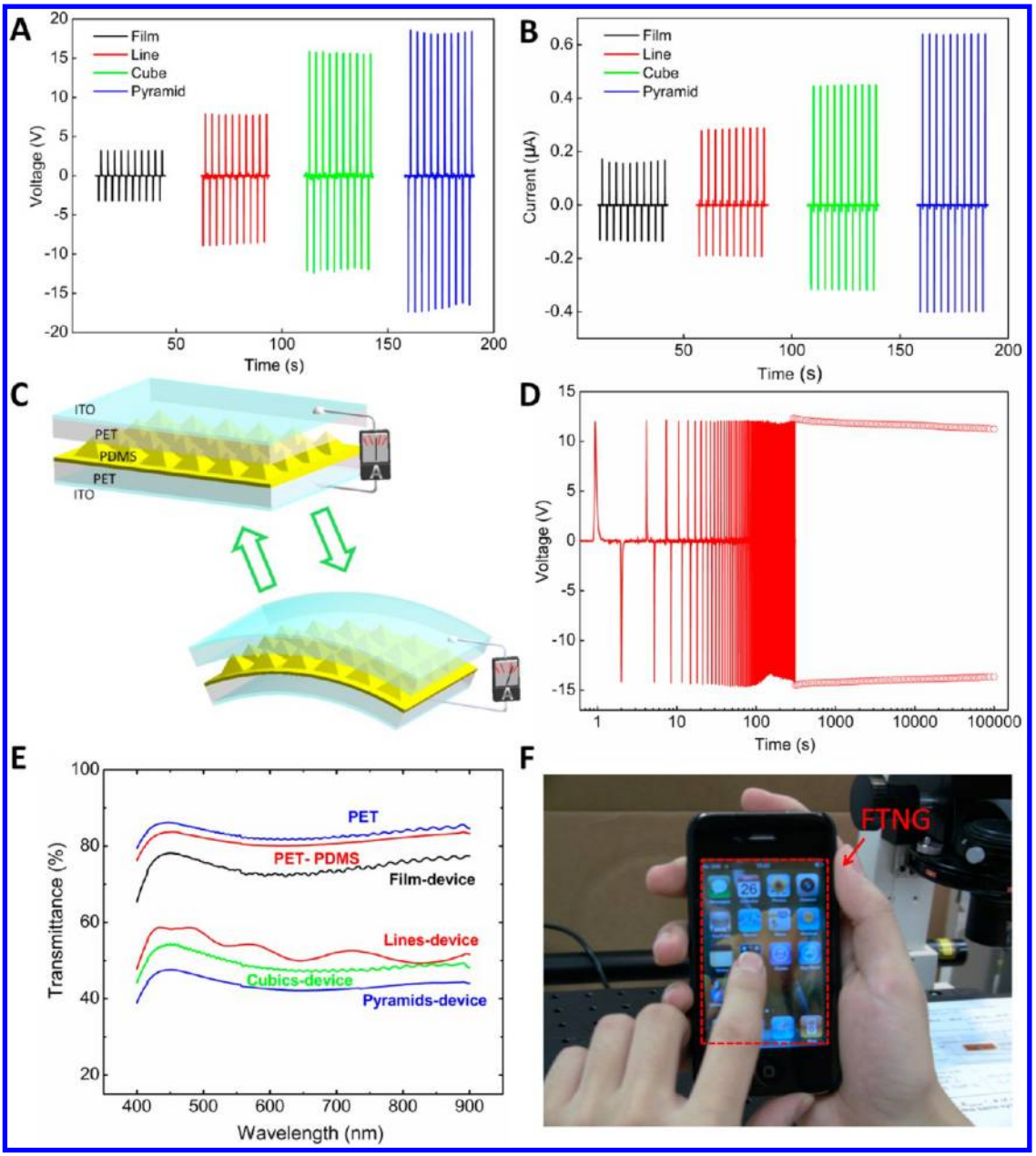

Figure 3. Electrical output and optical measurement of the FTNG. (A) Output voltage of the FTNG using PDMS thin film with flat surface and various patterned features, respectively. (B) Output current of the FTNG using PDMS thin film with flat surface and various patterned features, respectively. (C) Schematic illustration of the charge-generating process of the triboelectric generator. Pushed by the bending force from the linear motor, the device will be switching back and forth between the normal state (top-left) and the bending state (bottom-right), and there will be an alternating flow of electrons in the external circuit driven by the induced triboelectric potential. The detailed mechanism could be found in the Supporting Information. (D) Stability test for the FTNG. (E) The UV−vis spectra of various types of substrates and FTNG devices. (F) The photograph of a FTNG device attached on the screen of a smart phone that indicates the high transparency of the NG device.

sensor.[24,25] Figure 4A illustrates the voltage-output signal of various types of sensor devices to the applied pressure induced by a droplet of water (8 mg, ~3.6 Pa in pressure). All types of FTNGs have a high sensitivity and fast response to the external force and show as a sharp peak signal (Video S1 in Supporting Information). The sensitivities of the line-featured and cube-featured sensors were about five and ten times, respectively, larger than that of the unstructured film-featured sensor. The pyramid-featured device showed the highest sensitivity in the four types of pressure sensors, which is consistent with our results on the triboelectric generator and the previous report on plastic thin-film pressure sensors.[10] Furthermore, we measured the response to the impact of a piece of feather (20 mg, ~0.4 Pa in contact pressure, corresponding to a low-end detection limit of 13 mPa, see Supporting Information for the calculation of detection limit). In Figure 4B, the sensor shows two opposite voltage signal curves indicating the feather loading (on) and unloading (off) process. In the real situation, when the feather falls on the sensor, it will go through two processes: initially touching the sensor, and completely falling on the sensor. The sensor signal can delicately show these details of the entire process. The existing results show that our sensor can be applied for measuring the subtle pressure in real life.

dx.doi.org/10.1021/nl300988z | Nano Lett. XXXX, XXX, XXX−XXX

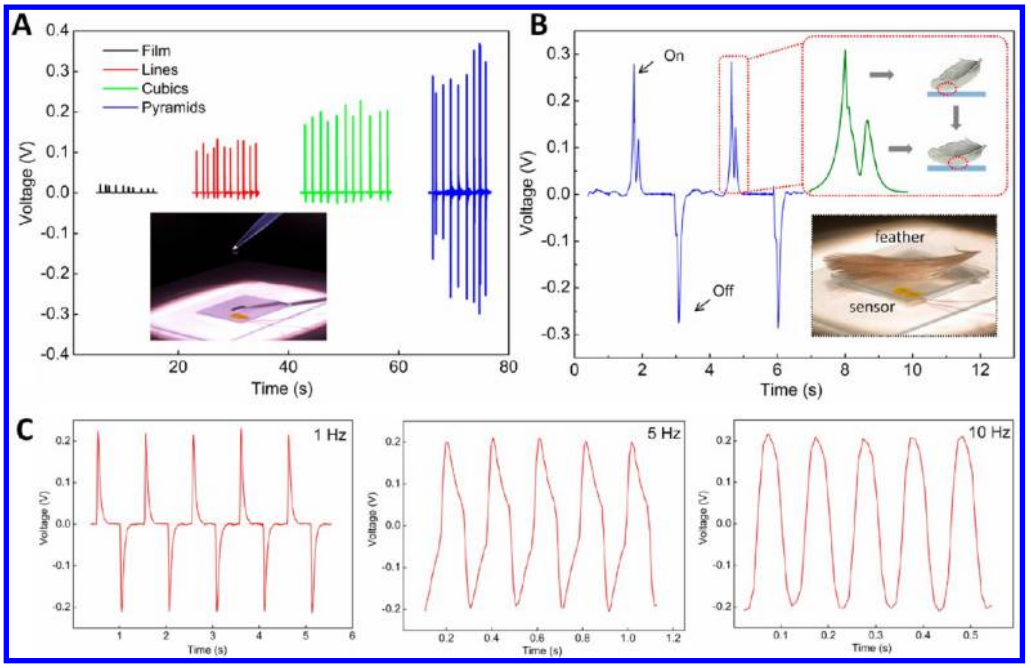

Figure 4. Characterization of the self-powered pressure sensor devices. (A) Performance of the pressure sensor device induced by a droplet of water falling from about 5 cm high. The voltage responses of various types of sensor devices were measured. (B) Performance of the pressure sensor device induced by a piece of feather. The top inset image illustrates the process that a double peak was induced by placement of the feather. The bottom inset image shows the photograph of the feather induced pressure sensor. (C) Measurement of the frequency characteristics of the pressure sensor. The linear motor was utilized to apply a tiny force to the pressure sensor device with different frequencies (1, 5, and 10 Hz, respectively), and the voltage response of the pressure sensor was measured.

Though having a similar structure, the sensor device described here has a different principle compared with another plastic pressure sensor reported by Bao's group.[10] First, our sensor is a self-powered device and based on the power generation rather than the capacitance change induced by pressure, which means that our sensor device is more accessible for measurement. Second, the response signal of our sensor is a sharp peak instead of a state curve, which exhibits a fast response and no hysteresis with the fast switching of the sensor. To illustrate this point, we measured the time-resolved response as a function of the frequency of the applied pressure (Figure 4C). We used a linear motor to exert a slight pressure to the sensor device with different frequencies of 1, 5, and 10 Hz. Clearly, the voltage output signal has no significant degradation up to 10 Hz, which demonstrates the fast and deterministic response of the pressure sensor.

In summary, we have demonstrated a new flexible transparent nanogenerator based on the triboelectric process and it can be used as a self-powered high-sensitive pressure sensor. Three types of regular and uniform PDMS patterned arrays at the micrometer scale are achieved through a common and scalable approach. This novel design can significantly improve the output efficiency of the nanogenerator by increasing the triboelectric effect and the capacitance change. For a typical FTNG with pyramid-featured PDMS pattern, the electrical output achieved a peak voltage of 18 V and current of 0.7 μA with a peak current density of ~0.13 μA/cm^2, which is four times as high as that of the previously reported triboelectric generator. As the entire structure of FTNG was fabricated by transparent polymer materials and electrode, the film-featured devices show transparency of ~75%, resulting in a transparent flexible nanogenerator. Further, owing to the simple and low-cost production process, the FTNG exhibits great advantages in industrial production and practical applications as well as manufacturability, durability, and capability of integration with other processing technologies. Finally, the FTNG shows its potential application in self-powered systems for touchscreens, electronic displays, and even personal electronics.

Methods. *Fabrication of FTNGs and Pressure Sensors.* To make patterned Si molds, 4 in. (100) Si wafers were patterned using photolithography. The patterned wafers were etched anisotropically using a dry etching process, resulting in the formation of recessed pyramids, and etched isotropically using a wet etching process to fabricate recessed line and cubic features. After cleaned with acetone and isopropanol, all of the Si masters were treated with trimethylchlorosilane (Sigma Aldrich) by gas phase silanization to avoid the adhesion between PDMS and Si molds. In preparing the patterned polymer films, PDMS elastomer and cross-linker (Sylgard 184, Tow Corning) were mixed in a 10:1 ratio (w/w), and then casted on the Si masters. After a degassed process under vacuum, the elastomer mixture was spin-coated at 500 rpm for 60 s (SCS 6800 spin coater, Specialty Coating System). After incubated at 85 °C for 1 h, a uniform PDMS thin film was peeled off from Si mold and then placed on uncured PDMS on a piece of clean ITO-coated PET film (Sigma Aldrich), followed by curing at 85 °C for 8 h. Finally, another clean ITO-coated PET film was placed onto the prepared PDMS-PET substrate to form a sandwiched structure. Therefore, both of the top and bottom surfaces of this structure were covered with a thin conductive ITO layer. The two short edges of the device were sealed with ordinary adhesive tape to ensure an adequate contact between PET and patterned PDMS films. To make a full FTNG device, silver paste was applied to connect the ITO electrodes to the copper conducting wires. The effective size of the FTNG was 4.5 cm × 1.2 cm, and the total thickness of the

dx.doi.org/10.1021/nl300988z | *Nano Lett.* XXXX, XXX, XXX−XXX

device is about 460 μm. The fabrication of the pressure sensor devices was similar to that of the FTNG devices except that the shape of the pressure sensor devices was square and the effective size was 3 cm × 3 cm.

Electrical Output, Mechanical and Optical Measurements. For the measurement of the electrical output of the FTNG, an external force was applied to make the device bending by a commercial linear mechanical motor, and there would be friction between the patterned PDMS thin film and top PET layer, resulting in triboelectric potential and electrical output in the external circuit (Supporting Information Figure S2). The output voltage and current were measured by Keithley 6514 System Electrometer and SR570 low noise current amplifier from Stanford Research Systems, respectively. To test the mechanical stability and robustness of the FTNG, the whole device withstood >100 000 nonstop bending cycles at a frequency of 1 Hz. The working mechanism and measurement procedure of the pressure sensor devices were similar to those of the FTNG devices. Some tiny objectives such as a droplet of distilled water, a small piece of paper, and even a piece of bird feather were utilized to induce pressure upon the device. The obtained response of voltage peak was measured by SR560 preamplifier from Stanford Research Systems. The transmittance of the device was measured by UV−vis spectroscopy method with Beckman DU 640 spectrophotometer. The atmosphere is used as the reference. The FTNG devices with both nonpatterned and various types of patterned PDMS thin films were measured. All of the testing was carried out in an ambient environment at room temperature.

■ ASSOCIATED CONTENT

Supporting Information

Additional figures showing the principle and strategy of this work, the detailed mechanism, SEM images of the patterned PDMS film with smaller features, and a video on the applications of the pressure sensor. This material is available free of charge via the Internet at http://pubs.acs.org.

■ AUTHOR INFORMATION

Corresponding Author

*E-mail: zhong.wang@mse.gatech.edu.

Author Contributions

‖These authors contributed equally to the work.

Notes

The authors declare no competing financial interest.

■ ACKNOWLEDGMENTS

This research was supported by BES, DOE, and NSF, MURI from Airforce, and the Knowledge Innovation Program of Chinese Academy of Sciences (KJCX2-YW-M13). The authors would like to thank Dr. Yan Zhang, Wenxi Guo, and Sihong Wang for helpful discussions and assistance in the experiments.

■ REFERENCES

(1) Menard, E.; Meitl, M. A.; Sun, Y. G.; Park, J.-U.; Shir, D. J.-L.; Nam, Y.-S.; Jeon, S.; Rogers, J. A. *Chem. Rev.* **2007**, *107*, 1117−1160.

(2) Ko, H. C.; Stoykovich, M. K.; Song, J. Z.; Malyarchuk, V.; Choi, W. M.; Yu, C.-J.; Geddes, L. B.; Xiao, J. L.; Wang, S. D.; Huang, Y. G.; Rogers, J. A. *Nature* **2008**, *454*, 748−753.

(3) Kim, D.-H.; Lu, N. S.; Ma, R.; Kim, Y.-S.; Kim, R.-H.; Wang, S. D.; Wu, J.; Won, S. M.; Tao, H.; Islam, A.; Yu, K. J.; Kim, T.-I.; Chowdhury, R.; Ying, M.; Xu, L. Z.; Li, M.; Chung, H.-J.; Keum, H.; McCormick, M.; Liu, P.; Zhang, Y.-W.; Omenetto, F. G.; Huang, Y. G.; Coleman, T.; Rogers, J. A. *Science* **2011**, *333*, 838−843.

(4) Artukovic, E.; Kaempgen, M.; Hecht, D. S.; Roth, S.; Grüner, G. *Nano Lett.* **2005**, *5*, 757−760.

(5) Sanghyun, J.; Facchetti, A.; Xuan, Y.; Liu, J.; Ishikawa, F.; Ye, P. D.; Zhou, C. W.; Marks, T. J.; Janes, D. B. *Nat. Nanotechnol.* **2007**, *2*, 378−384.

(6) Yang, Y.; Jeong, S.; Hu, L. B.; Wu, H.; Lee, S. W.; Cui, Y. *Proc. Natl. Acad. Sci. U.S.A.* **2011**, *108*, 13013−13018.

(7) Chen, P. C.; Shen, G. Z.; Sukcharoenchoke, S.; Zhou, C. W. *Appl. Phys. Lett.* **2009**, *94*, 043113−043115.

(8) Ge, J.; Cheng, G. H.; Chen, L. W. *Nanoscale* **2011**, *3*, 3084−3088.

(9) Someya, T.; Sekitani, T.; Iba, S.; Kata, Y.; Kawaguchi, H.; Sakurai, T. *Proc. Natl. Acad. Sci. U.S.A.* **2004**, *101*, 9966−9970.

(10) Mannsfeld, S. C. B.; Tee, B. C.-K.; Stoltenberg, R. M.; Chen, C. V. H-H.; Barman, S.; Muir, B. V. O.; Sokolov, A. N.; Reese, C.; Bao, Z. N. *Nat. Mater.* **2010**, *9*, 859−864.

(11) Takei, K.; Takahashi, T.; Ho, J. C.; Ko, H.; Gillies, A. G.; Leu, P. W.; Fearing, R. S.; Javey, A. *Nat. Mater.* **2010**, *9*, 821−826.

(12) Lipomi, D. J.; Vosgueritchian, M.; Tee, B. C-K.; Hellstrom, S. L.; Lee, J. A.; Fox, C. H.; Bao, Z. N. *Nat. Nanotechnol* **2011**, *6*, 788−792.

(13) Wang, Z. L.; Song, J. H. *Science* **2006**, *312*, 242−246.

(14) Wang, X. D.; Song, J. H.; Liu, J.; Wang, Z. L. *Science* **2007**, *316*, 102−105.

(15) Qin, Y.; Wang, X. D.; Wang, Z. L. *Nature* **2008**, *451*, 809−813.

(16) Wang, Z. L. Nanogenerators for self-powered devices and systems; *SMARTech* digital repository, Georgia Institute of Technology: Atlanta, GA, 2011.

(17) Wang, X. D. *Nano Energy* **2012**, *1*, 13−24.

(18) Choi, M.-Y.; Choi, D.; Jin, M.-J.; Kim, I.; Kim, S.-H.; Choi, J.-Y.; Lee, S. Y.; Kim, J. M.; Kim, S.-W. *Adv. Mater.* **2009**, *21*, 2185−2189.

(19) Choi, D.; Choi, M.-Y.; Choi, W. M.; Shin, H. J.; Park, H.-K.; Seo, J.-S.; Park, J.; Yoon, S.-M.; Chae, S. J.; Lee, Y. H.; Kim, S.-W.; Choi, J.-Y.; Lee, S. Y.; Kim, J. M. *Adv. Mater.* **2010**, *22*, 2187−2192.

(20) Choi, D.; Choi, M.-Y.; Shin, H.-J.; Yoon, S.-M.; Seo, J.-S.; Choi, J.-Y.; Lee, S. Y.; Kim, J. M.; Kim, S.-W. *J. Phys. Chem. C* **2010**, *114*, 1379−1384.

(21) Park, H.-K.; Lee, K. Y.; Seo, J.-S.; Jeong, J.-A.; Kim, H.-K.; Choi, D.; Kim, S.-W. *Adv. Funct. Mater.* **2011**, *21*, 1187−1193.

(22) Fan, F. R.; Tian, Z. Q.; Wang, Z. L. *Nano Energy* **2012**, *1*, 328−334.

(23) Weibel, D. B.; DiLuzio, W. R.; Whitesides, G. M. *Nat. Rev. Microbiol.* **2007**, *5*, 209−218.

(24) Li, Z. T.; Wang, Z. L. *Adv. Mater.* **2011**, *23*, 84−89.

(25) Wang, Z. L. *Adv. Mater.* **2012**, *24*, 280−285.